A STUDY OF STRUCTURE AND ELECTRICAL RESISTIVITY OF THE SUPERCONDUCTOR $Pr_{1.85}Ce_{0.15}Cu_{1-x}Ni_xO_4$

DISSERTATION

Submitted for the award of the degree of

Master of Philosophy

in

PHYSICS

BY

ARFAT FIRDOUS

under the supervision of

PROF. J. P. SRIVASTAVA

DEPARTMENT OF PHYSICS
ALIGARH MUSLIM UNIVERSITY
ALIGARH (INDIA)

2004

Dedicated
to Pyari, Haleema, Imran Firdousi
and my late Friend
Ashfaque Saleem.

DEPARTMENT OF PHYSICS
ALIGARH MUSLIM UNIVERSITY
ALIGARH-202002 (U.P) INDIA
Phone No.0091-571-2701001

Certificate

Certified that the work presented in the M. Phil. dissertation entitled **"A Study of Structure and Electrical Resistivity of the Superconductor $Pr_{1.85}Ce_{0.15}Cu_{1-x}Ni_xO_4$"** is the original work of Mr. Arfat Firdous, carried out under my supervision.

31.3.2004
(Prof. J. P. Srivastava)

Acknowledgements

The credibility to compile my M.Phil work goes to my supervisor Prof.J.P.Srivastava.I appreciate his consistent and legitimate principles, which really work for any candidate. I admit my deep respect and gratitude to him for his inspiring guidance and keen interest during my research work.

I am also thankful of my ex-supervisor Dr.S.Mollah for his kind contribution in my course work.

It is my pleasure to thank Chairman, Prof. A.K.Chaubey, Prof. Rahimullah Khan and Prof. R. P. Mathur former Chairman of the Department of Physics for their official help at the appropriate times.

It is my pleasant duty to thank my colleague Mohd. Wasi Khan for assisting me in understanding the computer software.

Finally, I feel sincerely thankful to all my friends and senior colleagues, especially, Dr.Shahid Hussain, Dr. Abbas Ali and Mr.S.H.Shahid Rizvi for their close association and encouragement.

(ARFAT FIRDOUS)

Contents

Introduction

Introduction

After the discovery of electron-doped superconductors with the chemical formula $Ln_{2-x}M_xCuO_{4-y}$ where Ln is a rare earth (Ln=Nd, Sm, Pr and Eu) and M is tertravalent (M=Ce, Th) the correlation between Ce and the superconducting properties has been extensively investigated [1, 2]. The discovery of electron type superconductivity has particularly interesting implications in view of the fact that in the previously known high T_c materials the charge carriers are considered to be holes. The mechanism of superconductivity in these materials is very complex and the charge carriers are created by substitution of trivalent rare earth ion with tetravalent Ce.This subsequently results in the removal of oxygen. The oxygen stoichiometry plays a prominent role and hence the superconducting transition occurs only after annealing under reduced atmosphere.

These compounds crystallize in Ln_2CuO_{4-y} (Ln= Nd, Pr, Sm, and Eu) T´-structure, space group I4/mmm and superconductivity is frequently met in Ce or Th doping modes. The T´-type structure differs from the tetragonal structure. In former the rare earth, Cu, and one set of oxygen atoms are in similar positions, but a second set of oxygens are in sites above and below the oxygens in the CuO_2 planes instead of apical positions occupied in hole doped structures.

The maximum superconducting critical temperature around 25K is observed in a Ce or Th doped systems at about x=0.15 and y=0.02 [3]. Also several experiments have demonstrated that the concentration range of Ce or Th within which superconductivity occurs in electron-doped compounds is

much narrower ($0.10 \leq x \leq 0.18$) than that of hole doped $La_{2-x}Sr_xCuO_{4-y}$ systems ($0.05 \leq x \leq 0.30$)[4]. Recently, Brinkman et al. [5] have proposed that the bulk superconductivity can be found in $Pr_{2-x}Ce_xCuO_{4-y}$ single crystals over a wide concentration range ($0.04 \leq x \leq 0.17$). The origin of such an extended range is a consequence of the reduction process at a high temperature of 1100°C. The involvement of cationic and anionic inhomogeneities in electron-doped superconductors is rather complex. It has been claimed that there are at least two important variables, the effectiveness of cerium diffusion during the sintering and oxygen removal during the reduction process.

Peng et al. [6] have investigated structural, magnetic and transport properties of crystalline $Pr_{2-x}Ce_xCuO_{4-y}$ ($0.0 \leq x \leq 0.24$) thin films prepared by pulsed laser deposition. They observed that the superconductivity occurs within a narrow concentration range of Ce ($0.13 \leq x \leq 0.18$), similar to one found in polycrystalline samples. It was argued that the large extended range found by Brinkman et al. [7] was linked to: (1) Ce inhomogeneity of the crystal (2) inhomogeneous reduction of the crystal. Maiser et al. [8] investigated the superconducting properties of thin films of these compounds between "0.0 to 0.24" subjected to heating at different temperatures including high temperature annealing performed by Brinkman. It was found that the reduction process at high temperatures result in the increase of both free carriers and inhomogeneity of all the samples without inducing bulk superconductivity with $x \leq 0.10$. It was suggested that the reduction process involves the removal of oxygen from the sites other than apical one in T′-structure.

Magnetic susceptibility and electron paramagnetic resonance measurements on polycrystalline samples have been reported by Saez Puche and coworkers, who concluded that the Cu moments are ordered antiferromagnetically below 300K[9].

Transport measurements have shown that there is a metal-insulator crossover as a function of Ce doping in the normal state of electron-doped cuprate [10].

Although the diamagnetic Meissner effect is one of the defining properties of a superconductor, an unusual paramagnetic response is sometimes observed in these samples when cooled in a weak magnetic field below critical temperature T_c [11]. In high temperature superconductors the paramagnetic Meissner effect is argued to be a consequence of the d-wave pairing [12].

Superconductors have tremendous potential for application. It is extremely advantageous to use them as conductors of electric current because of their nondissipative property. The main applications are: high field magnets, supercurrent quantum interference devices, sensors, etc. In addition to being employed in SQUIDS, there are a large number of applications of Josephson junctions in electronic circuitry.

In the light of these reports we undertook the synthesis of a series of $Pr_{1.85}Ce_{0.15}Cu_{1-x}Ni_xO_4$ .The aim of Ni doping is to observe the effect of a ferromagnetic material in the superconducting matrix at copper sites. In the present work a systematic study of structural and the transport properties of $Pr_{1.85}Ce_{0.15}Cu_{1-x}Ni_xO_4$ (x=0.0025, 0.005,0.0075,0.01,) has been undertaken. The changes in the structural and transport properties of the $Pr_{1.85}Ce_{0.15}CuO_4$ with varying Ni concentration have been

investigated. It is found that the transition temperature falls substantially at x=0.0025, 0.0050. However, at x=0.0075,0.0100 the superconducting phase is destroyed.

Our higher temperature resistivity data fit well in the Mott's variable range hopping (VRH) model in these materials. The fit shows that the slopes of the curves first decrease with the increase of Ni concentration for x = 0.0025, 0.005 and then increase for x = 0.0075 and 0.01. Accordingly, the activation energy (E_c) also first decreases and then increases. . The increase and decrease of activation energy can explain the resistivity of the samples.

Chapter I

Brief Historical and Theoretical view of Superconductors

Brief History of Superconductors

After the Kammerling Onnes's discovery of superconductivity in 1911 many new materials were investigated for superconductivity. But the quest for high transition temperature (T_c) yielded no noticeable returns till 1986 and the highest value T_c could touch was only 25K for Nb_3Ge. The picture changed radically with the discovery of Bednorz and Müller in 1986, who found that Ba doped La_2CuO_4 at the dopant concentration of about 8% becomes a superconductor with T_c~35K[13]. The thirst has always remained there as a challenge for scientists to discover a superconductor, which can conduct at the room temperature. This dream still seems far away. But vigorous efforts to discover a room temperature superconductor are in process.

The next break-through was made by Chu's group in 1987 reporting T_c in the vicinity of 90K in a new material, $YBa_2Cu_3O_{7-x}$ [14]. Some new classes of copper oxide based materials have been discovered recently in a particular series of the system $Bi_2\ Sr_2\ Ca_{n-1}Cu_nO_{2n+4}$ with transition temperature 10K, 85K and 110K for n=1,2 and 3 respectively and in the series of $Tl_2Ba_2Ca_{n-1}Cu_nO_{2n+4}$ with the transition temperatures 80K, 110k, 125K for n=1,2,3 respectively [15]. In both these systems T_c increases with number n of CuO_2 planes per unit cell, at least in the range n=1,2,3.This led to a suggestion that the further increase in n may provide a route to higher T_c. But copper based materials may not be the only route to higher T_c.

All copper oxide based high transition temperature superconductors are highly anisotropic. They are tetragonal or nearly

tetragonal with slight orthorhombic distortion. The identification of HTS is carried out through the following investigations:

1. Crystal structure.
2. Meissner effect.
3. Resistivity.

1.1 Proposed theoretical Models

We describe below in brief some of the models that have been applied to interpret the transport properties of the type of material studied by us.

- **Resonant Valence Bonds (RVB) Model**

Anderson and Pauling proposed this model under the roof of magnetic interactions [16]. It was observed by Anderson that all the superconductors of this new class occur near a metal to insulator transition. This transition is perhaps a Mott-Transition and occurs in an odd electron insulator state. Moreover, this state has peculiar magnetic properties. It has been pointed out that the most copper oxide including $YBa_2Cu_2O_5$, are Mott insulators [17]. A Mott transition involves conversion of metal into so-called Mott insulator when the inter-atomic spacing exceeds a certain critical value. Anderson's 1973 article originally proposed the RVB state for triangular lattice and extended this to the two-dimensional square lattice [18], appropriate for Cu-O planes. The relevant Hamiltonian is a second order Heisenberg type

$$H=-J\sum b_{ij}^{\dagger}b_{ij} \quad \text{.....(1.1)}$$

with $J=4t^2/U$.....(1.2)

and U>t, where t is Mott-Hubard parameter, representing the electron-hopping matrix and U represents the electron-electron correlation energy. The second quantization operator $b_{ij}^{\dagger}$ creates and its counterpart b_{ij} destroys a valence-bonded pair respectively. The RVB is related to fractional quantum Hall effect Laughlin states and the state ϕ_{RVB} is given by

$$\phi_{RVB} = \int d\theta \exp(-iN/2\theta)\pi\ \phi_0/(1+\alpha k^2)\ [1+\exp i\theta a_k b_{k+}] \quad \text{.....(1.3)}$$

The RVB state can be thought of as a Bose condensate of Cooper pairs of neutral solitons[19]. Physically each atom is bonded to one neighboring atom by single electron pair and the ground state is the linear coherent superposition of all the states that can be formed by such a dimerization of lattice[20].

The RVB ground state is not the conventional antiferromagnetic or Neel type. When one or both of the following conditions are satisfied; (a) the next neighbour coupling is antiferromagnetic (b) there are virtual phonon interactions, short of being strong enough to excite a spin-Peierls instability [16]. However, experimentally the copper oxide systems seem to exhibit a long-range antiferromagnetic order as opposite to the RVB dimerization. Peierls instability involves the formation of an energy gap at the Fermi surface of a linear metal, due to its instability with respect to the static lattice deformation of wave vector $2k_F$.

There is a gap in energy for any charged excitation of RVB bond state with Fermi energy in the gap for the stoichiometric compound, and hence this half-filled compound is an insulator. Doping removes the "half-filled" scheme by removing electron pairs. The singly charged vacancies can be formed in pairs. These vacancies will be bosons with the charge "e",that is, the system is a Bose-condensate of charged solitons. One kind of the lowest excitation is spin excitation which is a neutral soliton or half-spin, charge zero particle.

The RVB also involves a Bose condensate of Cooper pairs of neutral solitons with a gap in energy $E_g=2\Delta$, where E_g is the energy needed to break a bond. The zero spin charged bosons in the Bose condensate may be mobile enough to carry the current. In this model the mechanism of superconductivity is predominantly electronic and magnetic, although weak phonon interactions may favour the RVB state.

Following are the predictions of the model, which are compatible with several measurable quantities.

I. The absence of gaps.
II. Antiferromagnetic or insulating behaviour of undoped or weakly doped Cu-O compounds.
III. The absence of an isotopic effect, low temperature specific heat and elastic properties dominated by electronic energies.
IV. Temperature dependence of normal state resistivity and the carrier density versus Hall-Seebeck coefficients.

Calculations of the ratio of E_g/kT_c for the RVB state seem to indicate a small value compared with the BCS prediction of 3.53.

Pauling[16] agrees that the mechanism of superconductivity is predominantly electronic and magnetic, although weak phonon interactions may favour the RVB state. Sufficiently strong doping transforms preexisting magnetic singlet pairs into charged superconducting pairs. Lines of alternating Cu-O atoms interacting with the layers of La and other cations give rise to the superconductivity. There is some resonance of $2Cu^{2+}$ to $Cu^{+} + Cu^{3+}$. The possibility of unsynchronized resonance when some oxygen atoms are missing stabilizes the conducting state. Other substances have favourable individual structural features, but only copper oxide superconductors comprise all of them. The superconducting behaviour of oxides has also been interpreted in terms of charge transfer resonance [21].

- **Antiferromagnetic Models**

Emery [22] model of La_2CuO_4 has an antiferromagnetic insulating limit. The holes reside in O-2p states and not in Cu-3d states because the short-range repulsion is better screened by oxygen than that by the copper. Strong coupling to local spins on the copper sites produces the pairing. This mechanism does not involve the much-discussed Cu^{3+}states [17]. The simultaneous presence of antiferromagnatism and superconducting states has been calculated using the related model [23].

The Emery model provides large estimate of T_c despite the possibility that the intermolecular vibrations can renormalize the parameters t, U and restrict T_c. Another criticism is that the highest T_c values are observed in orthorhombic YBaCuO, while the models consider the square planar coordination of tetragonal symmetry. Therefore, these models may not be sufficiently realistic. The justification for the antiferromagnetic model is

indicated by the experimentally observed antiferromagnetism in many oxide superconductors, the isotopic effect results do not support strong phonon coupling, and there is an observed gap in contrast to the expectations of the resonance models [24].

We have interpreted our resistivity data above T_c in the framework of the Variable Range Hopping Model whose application has been extremely successful in explaining the transition to the insulating states. The salient features of this model are sketched below.

1.1.1 Variable Range Hopping model

The theory of variable range hopping (VRH) has been quite successful in describing the conductivity in insulating samples. The original idea was given by Mott [25], with notable additions by Ambegaokar, Halperin and Langer [26], who formulated an approach using ideas from percolation theory. It is this approach, which will be sketched out in this section. A good discussion of Mott's original approach also appears in the book of Shklovskii and Efros [27].

The model concerns randomly placed single electron localized states with a spread in the single site binding energies. Conduction is assumed to occur by electrons hopping from site to site, the energy difference between the sites involved in the hop being supplied by phonons. Miller and Abrahams [28] considered such a system in which the electron wavefunctions were hydrogenic. Transition rates for electrons hopping from site i to site j were calculated. When a small electric field is applied, a current is produced which is proportional to the field. By this procedure an

effective resistance between sites i and j, R_{ij}, can be defined. Miller and Abrahams proposed that the effective resistance R_{ij} is a function of two intersite quantities: the distance between two sites r_{ij} and the difference in energies of the two sites $|E_i - E_j|$ .The dependence of the effective resistance R_{ij} on the distance between sites is what might be expected from the overlap of two wavefunctions,

$$R_{ij}\alpha \exp(2r_{ij}/a_H) \quad \text{.....(1.4)}$$

where a_H is the Bohr radius of the hydrogenic wavefunction of the impurities. The dependence of R_{ij} on the energy of the electron states on sites i and j is more complex. In addition to depending on the difference in energy, E_j-E_i, the resistance also depends on the values of E_i and E_j relative to the Fermi level, E_F. This connection to the Fermi level appears because an electron must hop to an empty site; no double occupancy was considered in the model. The Miller and Anrahams expression can be written as

$$R_{ij}\alpha \exp(\varepsilon_{ij}/k_BT) \quad \text{.....(1.5)}$$

where $\varepsilon_{ij} = 1/2(|E_i - E_j| + |E_i - E_F| + |E_j - E_F|)$

A key feature in this model is the large range of resistances. For example, an insulating sample SEP with an electron concentration of $10^{18}/cm^3$ has an average nearest neighbour impurity spacing of $n^{1/8}$---100Å---$6a_H$. In this random system one would expect to frequently encounter nearest neighbour pairs with a separation, which differed by a factor of 2 on either side of the average separation. Thus a plausible range of nearest

neighbor distances is $3a_H$ to $12a_H$. This range in the model of Miller and Abrahams would then imply a spread in nearest neighbor resistances of e^{18} $\approx 10^{18}$.This huge range of the resistances provides a condition, which makes the problem solvable.

Ambegaokar, Halperin and Langer [26] derived an expression for the variable range hopping conductivity by envisioning a sample as a set of discrete sites connected by resistors. The value of these resistors is taken to be the Miller and Abrahams value for the effective intersite resistances R_{ij}. The conductivity for this system is derived by using ideas from percolation theory. The resistances are parametrized as

$$R_{ij} = R_0 \exp(x_{ij}) \quad \text{.....(1.6)}$$

and values of x_{ij} are assumed to be uniformly distributed from $-x_0$ to x_0. One picks a value x, where x is between $-x_0$ and x_0. All bonds with $x_{ij}<x$ are connected with the appropriate resistance $R_{ij} = R_0 \exp(x_{ij})$, while bonds for which $x_{ij}>x$ are not connected. The value of x is then increased until the critical value for percolation, x_c, is reached. This process is depicted in Fig.1.1 The condition of having all bonds connected represents the samples of interest. Clearly, one would like to know the conductivity of the model when $x = x_0$. However, the enormous range of resistances in the problem allows a critical simplifying assumption to be made. It is assumed that the conductivity of the sample at percolation is determined by the value of the resistance just added, $R_0 \exp(x_c)$. One envisions these critical resistors completing the final links between the clusters of high conductivity. The conductivity of these already formed clusters is high because they are

composed of resistors whose values are small compared to $R_0 \exp(x_c)$. Likewise, the resisters added after percolation, while x increases from x_c *to* x_0, are large compared to R_0 *exp*(x_c), and will do a negligible job of shunting the critical resistors. Thus if the conductivity, σ is controlled by the resisters added just at percolation, we can write

$$\sigma \propto \exp(-x_c) \quad \text{.....(1.7)}$$

For a disordered physical system, $x_{ij} = 2r_{ij}/a_H + \varepsilon_{ij}/k_B T$. A value of x then sets a maximum r_{ij} and maximum ε_{ij}, which the two sites can have, to the candidates for connection. Namely, $r_{max} = a_H x/2$ and $\varepsilon_{max} = k_B T x$. The average number of sites, N, which are within r_{max} of a given site and within ε_{max} of the Fermi energy, is given by

$$N = \frac{4\pi}{3} r_{\max}^3 \, 2g(E_F)\varepsilon_{\max} \quad \text{.....(1.8)}$$

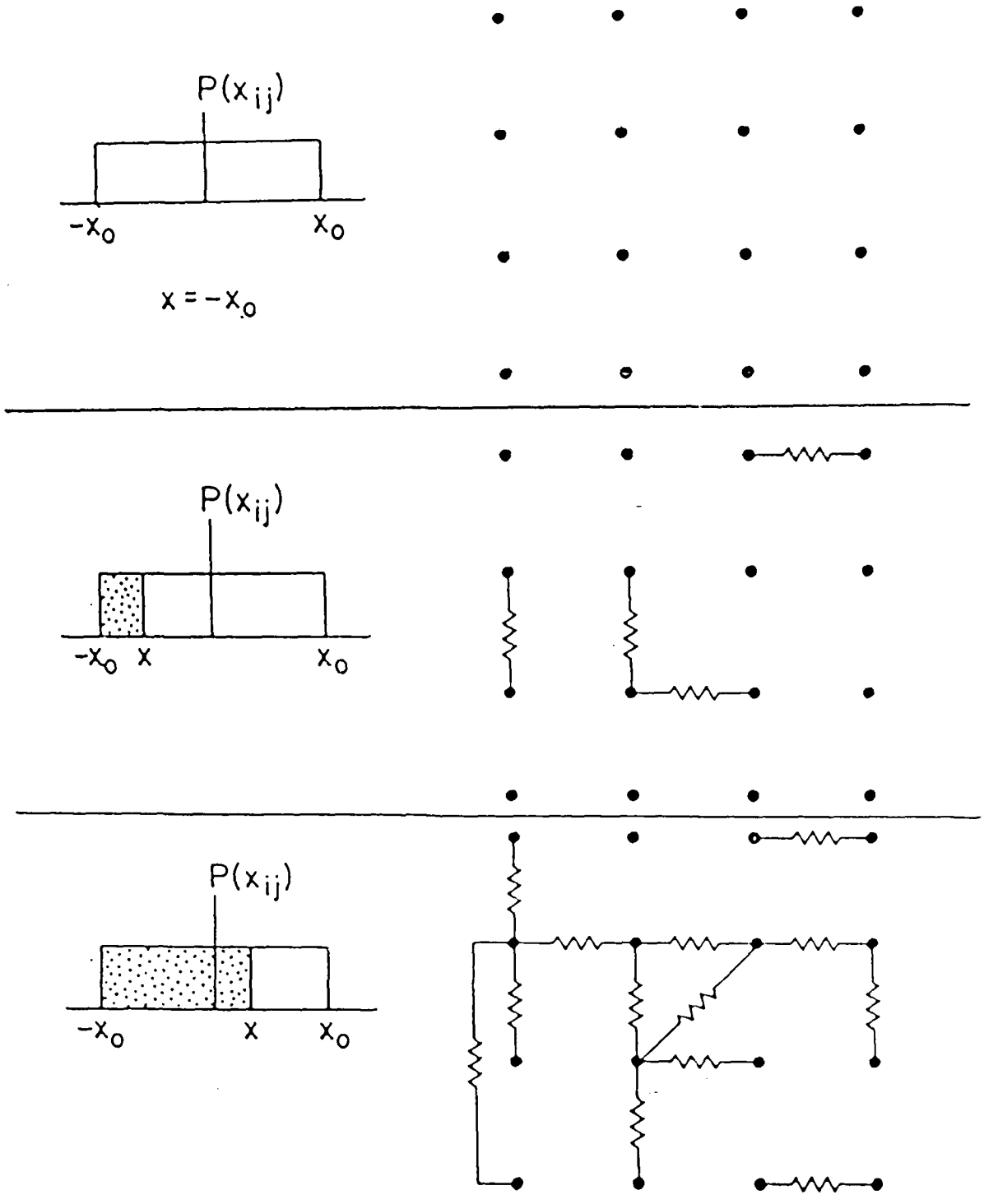

Figure 1.1 Depiction of the percolation process in a random resistor network. For each chosen value of x, all sites having a value of x_0 less than x are connected with a resistor of value $R_0 \exp(x_{ij})$. Sites having a value of x_{ij}>x are unconnected.

This expression has assumed a finite density of states at the Fermi energy, $g(E_F)$. The system percolates when $N=N_c$, which will be some number of the order of unity. Substituting the expressions for r_{max} and ε_{max} we obtain

$$N_c = \frac{\pi}{3} g(E_F) k_B T a_H^3 x_c^4 \quad \text{.....(1.9)}$$

From Eq. (1.7) we then get

$$\sigma(T) \propto \exp\left[-\left(\frac{3N_c}{\pi g(E) k_B a_H^3} \cdot \frac{1}{T}\right)^{1/4}\right] = \exp\left[-\left(\frac{T_0}{T}\right)^{1/4}\right] \quad \text{.....(1.10)}$$

This is the functional form for $\sigma(T)$ that describes the process known as variable range hopping (VRH).

To recapitulate, the main assumptions which lead to Eq. (1.10) are:

(i) Uncorrelated site energies. A hop from site i to an empty site j does not depend on whether a site close to j in space is occupied.

(ii) A constant density of states at the Fermi level. If $g(E_F)$ is nonzero, or not this should be a valid assumption at low temperature, where

ε_{max} becomes small. However, if $g(E_F)=0$, modifications to the VRH theory must be made.

Chapter II

Experimental Techniques

Introduction

This chapter deals with the method of preparation and characterization of samples, $Pr_{1.85}Ce_{0.15}Cu_{1-x}Ni_xO_4$ (x = 0.01, 0.0075, 0.005, 0.0025) used for the present study. We have adopted conventional solid-state reaction route. The Preparational details for having superconductivity in $Pr_{1.85}Ce_{0.15}Cu_{1-x}Ni_xO_4$ are more critical than in most of the hole doped high temperature superconductors. The oxygen concentration must be very close to the stoichiometric concentration; a little excess of oxygen rapidly quenches the superconductivity. The Ce concentration must also lie in a very narrow concentration range around x=0.15. Sol-gel precursor method is also used to synthesize the electron-doped superconductors to maintain the oxygen stoichiometry. The electron-doped superconductors have T´-type structure that differs from the tetragonal structure. In former the rare earth, Cu, and one set of oxygen atoms are in similar positions, but a second set of oxygens are in sites above and below the oxygens in the CuO_2 planes instead of apical positions occupied in hole doped structures shown in Fig.2.1

The techniques used to characterize these samples are described briefly below viz. *x*-ray diffraction (XRD), resistivity.

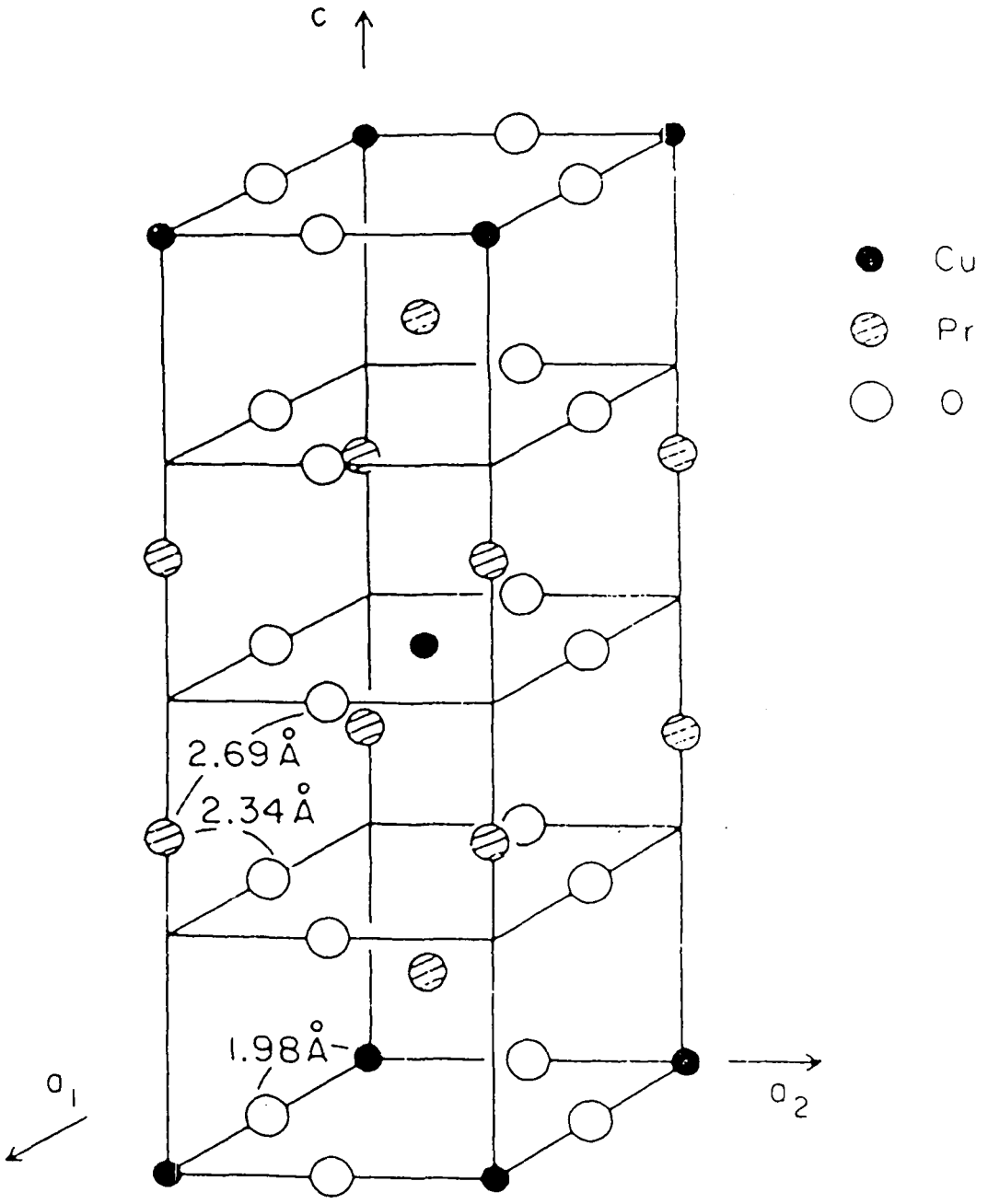

Fig.2.1 T´-type structure of Pr_2CuO_4.

Note the absence of oxygen at apical positions above and below the Cu atoms.

2.1 Synthesis of bulk samples

Generally, electron-doped superconductors are synthesized using solid-state reaction and sol-gel reaction routes. In the former method different constituents are mixed in stoichiometric ratio and heated at high temperatures under reduced atmosphere to complete the reaction.

We prepared the samples of $Pr_{1.85}Ce_{0.15}Cu_{1-x}Ni_xO_4$ (x = 0.01, 0.0075, 0.05, 0.0025) by the solid-state reaction method following the route shown in the flowchart Fig.2.2. The stoichiometric amounts of Pr_6O_{11}, CeO_2, CuO and NiO (all of AR grade) in powdered form were ground in an agate mortar till a homogeneous mixture was formed. This mixture was kept in a crucible and heated at 950°C for about 12 hours. The pre-sintered materials were again ground and calcinated at 950°C for 24 hours. The preheated powder was again ground with a few drops of polypine alcohol, which acts as a binder in the sample and pelletized using a rectangular die of dimension 14mmX4mmX2mm. A pressure of the order of 3 tons/cm^2 was used for making the pellet. Then, these pellets were annealed under reduced atmosphere at 850°C for 15 hours. The single-phase nature of the samples was studied using the powder *x*-ray diffraction technique.

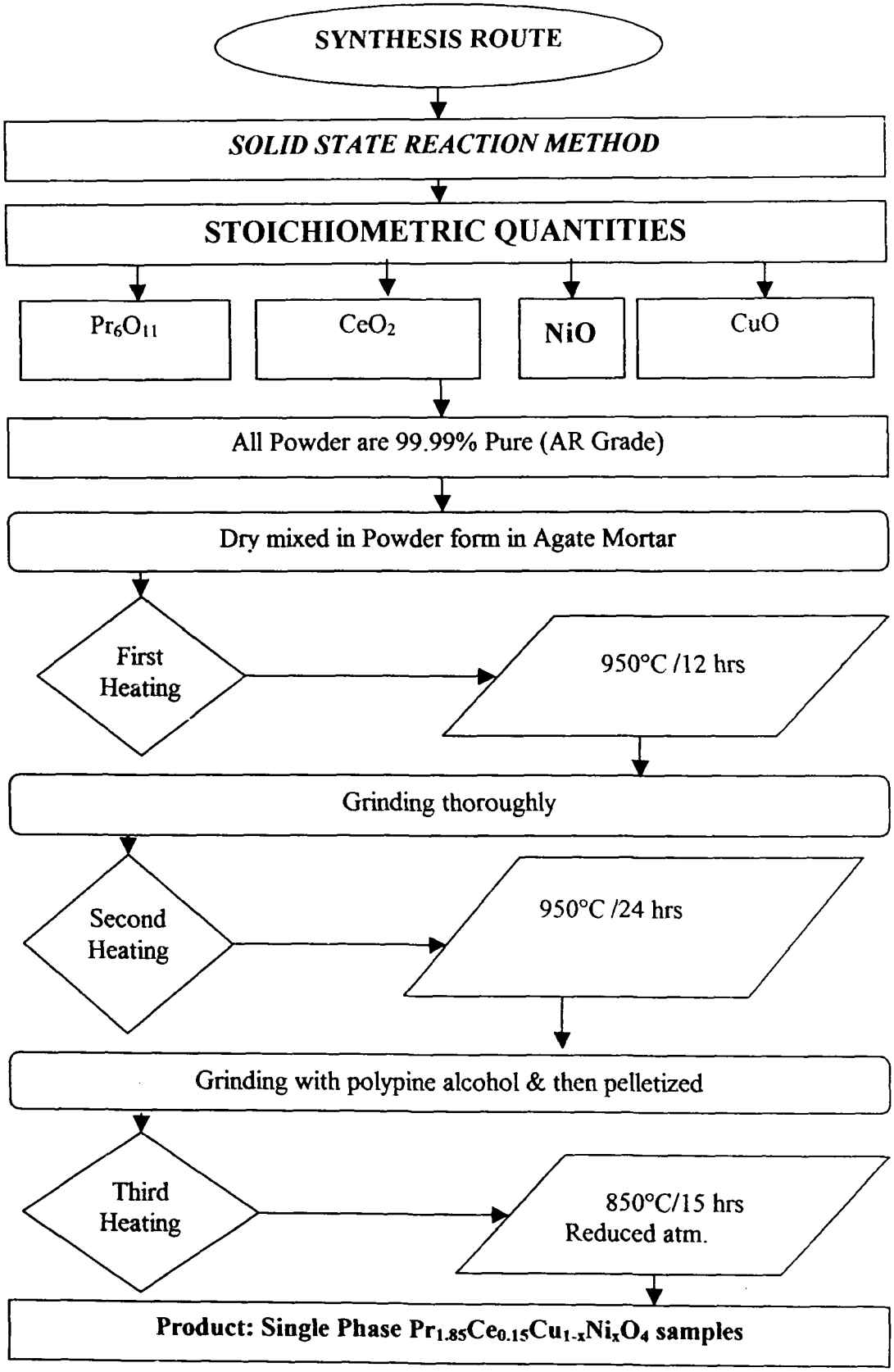

Fig. 2.2 Flow chart for solid-state reaction method used for synthesis of bulk samples.

2.2 X-ray diffraction

X-ray diffraction (XRD) is the most commonly used structural characterization for studying the samples in the powder form as well as in the thin film form. It is used to uniquely define the crystalline phases of the material, out of plane orientations of the thin film grain and relative in-plane alignments of the thin film with the substrate or between different layers in the case of the heterostructures. In normal θ-2θ scan mode, a beam of monochromatic *x*-rays is incident on the sample, making an angle θ with the sample surface. The detector motion is coupled with that of the *x*-ray source so that it is always kept at a position at an angle of 2θ with the incident direction of the *x*-ray beam. The recorded diffraction pattern gives the intensity versus 2θ plot. The XRD patterns were recorded with a diffractometer. The schematic of *x*-ray diffractometer is shown in Fig.2.3

The *x*-rays get diffracted from the crystal planes when the Bragg condition is satisfied. The condition is given by,

$$2d\sin\theta = n\lambda \quad \text{.....(2.1)}$$

where d is the interplanar spacing, n is the order of diffraction, λ is the wavelength of *x*-rays and θ is the incident glancing angle.

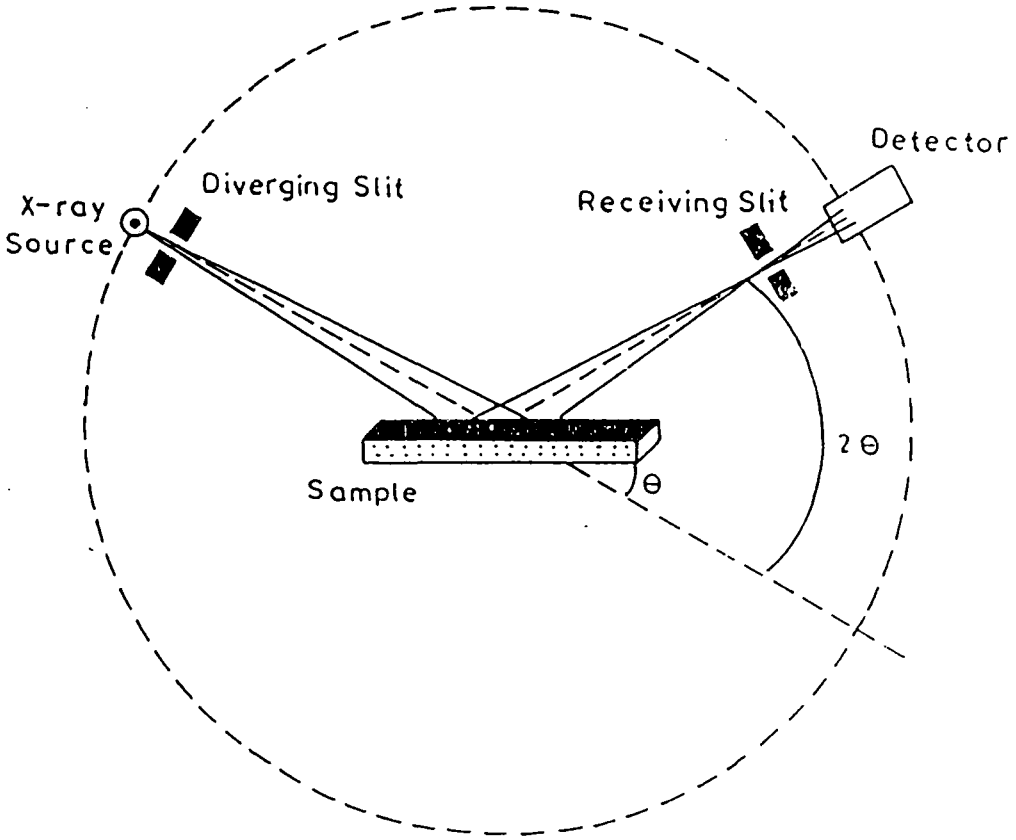

Fig. 2.3 The schematic of x-ray diffractometer.

This equation puts very stringent conditions on 'λ' and 'θ' for any given crystal. In order to satisfy the Bragg law either 'λ' or 'θ' can be varied, and this is done in different diffraction methods as follows:

	λ	θ
Laue method	Variable	Fixed
Rotating-crystal method	Fixed	Variable (over a range)
Powder method	Fixed	Variable

The structural analysis is carried out using *x*-rays of known wavelength λ. By measuring 2θ one can determine the spacing *d* between the planes of a certain family in the crystal. The diffraction pattern gives us information about the average particle/grain size, lattice parameters, crystal structure of the samples etc. The positions of atoms in the unit cell affect the intensities but not the directions of the diffracted beams. The intensity of the diffracted beam is changed by any change in atomic positions, conversely the atomic positions can be determined by the observations of diffracted intensities. It is interesting to understand the complex problem of relation between the atomic position and diffracted intensity. By measuring the shift in the

diffraction peak position, one can get an idea of the strain present in the sample.

The powder *x*-ray diffraction patterns have been recorded for the whole series of $Pr_{1.85}Ce_{0.15}Cu_{1-x}Ni_xO_4$ (x = 0.01, 0.0075, 0.05, 0.0025) at National Sun Yatsen University Tiwan using the Siemens diffractometer D5000 with Cu-K_α radiation (1.541838 Å) at room temperature. The cathode was maintained at 30 kV voltage. Diffraction patterns were recorded in the range $20^\circ \leq 2\theta \leq 80^\circ$. The lattice parameters have been determined using PowderX software. The indices could be assigned to all the lines on the basis of tetragonal symmetry. The structure refinement has been accomplished using the procedure developed by Rietveld [29, 30].

2.3 Brief History of Rietveld Refinement

The primary goal of this method is to refine crystal structures and profiles; hence it is called Rietveld method instead of 'profile refinement' or 'whole pattern fitting structure refinement'. It is called "Rietveld method", named after Dr. H. M. Rietveld . He was the first who worked out a computer based analytical procedure to make use of the full information content of the powder pattern and put it in public domain by publication of two seminal papers. He shared freely and widely his computer programme.

One of the great triumphs of Rietveld analysis has been in its crucial contributions to the development of the field of

high temperature superconductors. Experimentalists at some centers with the best diffraction facilities soon after the discovery of first genuine high T_c superconductot (T_c=90K) in 1987 at Brookhaven National Laboratory in the USA; the Rutherford-Appleton Laboratory in the UK and many other groups around the world studied larger samples of the polycrystalline matrix, performed Rietveld analysis with several different starting models, and all came to similar conclusions. The structure was correctly determined from the powder diffraction data whereas the *x*-ray single crystal results gave errors.

2.3.1 Structural analysis of the *x*-ray data

Fig.2.4 Shows the general approach to the structural analysis using XRD data, which has been employed in the present work. Structure refinement using the Rievtveld method is a powerful technique for extracting structural details from powder diffraction data. With present methods, structures with up to 200 structural parameters can be refined successfully, if care is taken and the data are of sufficiently high quality.

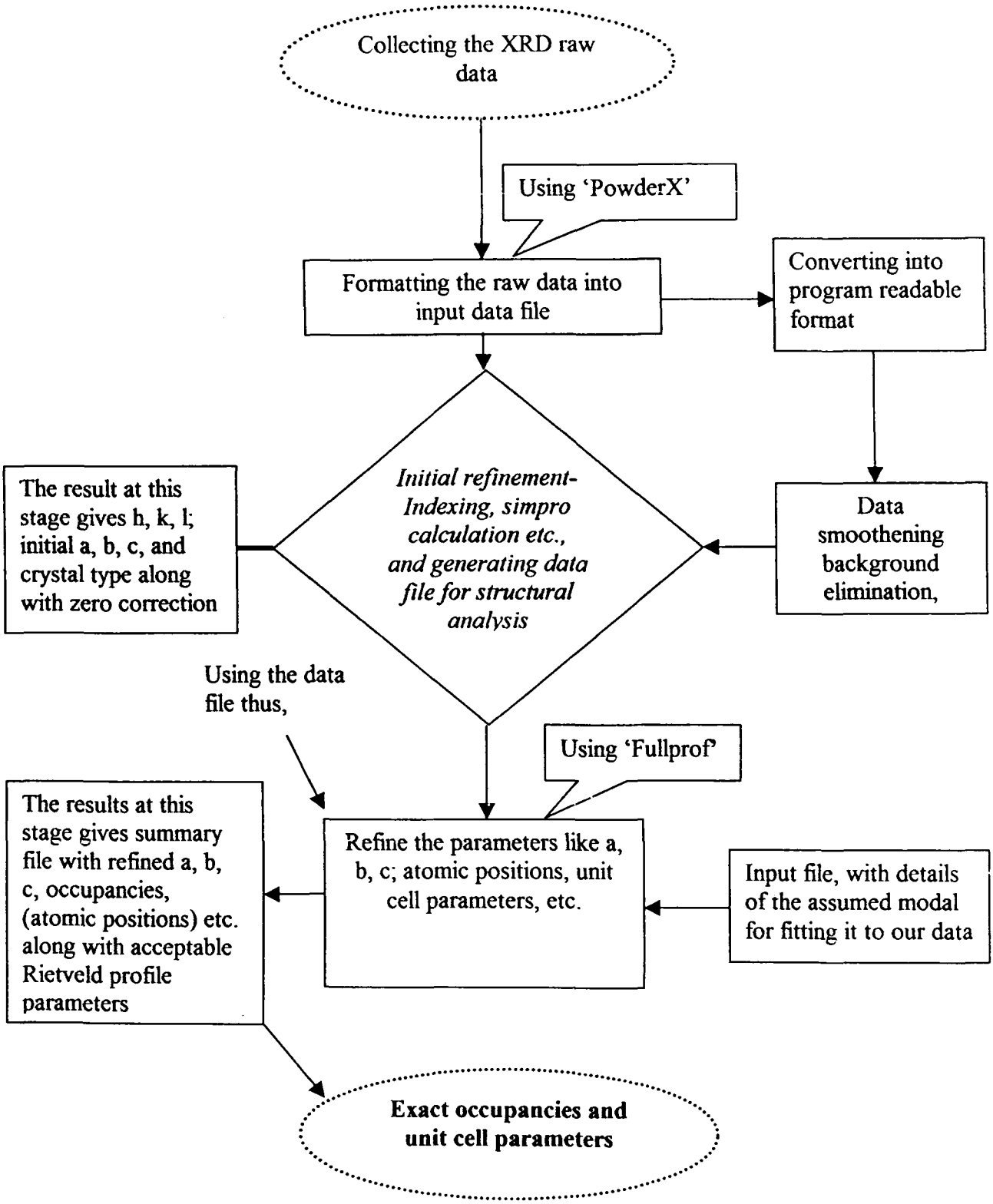

Fig. 2.4 Block –diagram for the analysis of XRD data.

The analysis of the *x*-ray data has been done using various computer softwares. Those used prominently in the present work are PowderX [31], FULLPROF [32]. We have used these softwares to obtain the unit cell parameters and site occupancies of all the polycrystalline samples studied.

2.3.2 PowderX

The general features of PowderX are summarized as:

- PowderX can read 13 data formats, from either angular-dispersive or energy dispersive *x*-ray diffraction, used in various diffractometers made by Mac Science, Philips, Siemens, Rigaku, etc. It can also write many data formats used for ab-initio structural solution and Rietveld refinements (EXPO, DBWS, GSAS, FULLPROF, RIETAN, etc.)
- It displays both the previous data and the data after processing so that it becomes very easy to see the effects of the processes during smoothening, background subtraction and 2 elimination.
- It offers a simple method for parameters input and it makes easy to use interfaces.
- It provides for various methods of data smoothening, 2 elimination and peak search are available, so that the user can find optimum method for his data set. The high-angle side fluctuation is less than 0.5% of the peak intensity in our method for Cu-K_2 elimination, which is much better than conventional Rachinger and Ladell method.

- Derivatives and Fourier transforms of the *x*-ray data can be calculated, plotted and saved as data files.
- Zero shift and other geometrical aberrations can be easily calculated and corrected.
- Any part of the plot can be zoomed with mouse to see the details.
- It prints the ready- to-publish plots of *x*-ray diffraction data.
- It edits the control file using graphical interfaces for pattern fitting programme Simpro.
- Several other programmes, d_{hkl} (the calculation of diffraction angles and crystal plane spacings from the lattice parameters), Lazy (generation of the simulated powder *x*-ray diffraction patterns), Treor90 (Index) and Eracel have been included in this system with user-friendly interfaces.

2.3.3 FULLPROF

Both *x*-ray and neutron diffraction data can be refined through Rietveld refinement programme. It is mainly used for Rietveld analysis (structure profile refinement) of neutron (CW, TOW, nuclear and magnetic scattering) or *x*-ray powder diffraction data collected as a function of the scattering variable T (2theta or TOF). The programme can be also used as a Profile Matching tool, without the knowledge of structure. Single crystal refinements can also be performed alone or in combination with powder data. The

programme FullProf is based on the code of the Young & Wiles (DBW) programme on the code DBW3.2S (Versions 8711 and 8804). The features of FullProf can be highlighted as:

- It provides for the choice of the line shape (Gaussian, Lorentzian, modified Lorentzians, pseudo-Voigt, Pearson-VII or Thomson-Cox-Hastings) for each phase.
- It can be used for both the neutron (constant wavelength and TOF) and *x*-ray (laboratory and synchrotron sources) data.
- It provides for the choice between automatic generation of hkl and/or symmetry operators and file given by user.
- Upto two wavelength (K_1+K_2) can be used for refinement.
- It has provision for the background refinement.
- Multiphase structure (upto 8 phases) can be refined.
- Preferred orientation: Two functions available.
- Absorption correction for a cylinder, microabsorption correction for flat samples can be made.
- There is a choice between three weighting schemes: standard least squares, maximum likelihood and unit weights.
- Magnetic structure refinement (crystallographic and spherical representation of the magnetic moments). The first method describes the magnetic structure in the crystallographic magnetic unit cell, making use of the propagation vectors. The second method is necessary for incommensurate magnetic structures.

- Automatic generation of reflections for an incommensurate structure with up to 24 propagation vectors. Refinement of propagation vectors in reciprocal lattice units.
- h, k, l dependence FWHM for strain and size effects.
- h, k, l dependence of shift and asymmetry for special kind of defects.
- Profile Matching: The full profile can be fitted without prior knowledge of the structure (needs only good starting cell and profile parameters).
- Quantitative analysis without the need of structure factor calculations.
- Chemical (distances) and magnetic (magnetic moments) slack constants.
- Resolution function (for pseudo-Voigt peak shape) may be supplied in a file.
- Structural or magnetic model could be supplied by an external subroutine for special purposes (rigid body, TLS, polymers, form factor refinements, small angle scattering of amphifilic crystals, description of incommensurate structures in real direct space, etc.)
- Single crystal data or integrated intensities can be used as observations (alone or in combination with a powder profile).

- Neutron (or *x*-ray) powder patterns can be mixed with integrated intensities of *x*-ray (or neutron) from single crystal or powder data.

The importance for using the FULLPROF programme is an input file, with the description (in proper format) of the assumed structure such as space group, atomic positions, occupancy, unit cell parameters etc. The programme generates a profile of the assumed structure (or say model) using the description we have provided. This pattern is refined to fit the observed data. By varying the profile generating parameters in the assumed model, a perfect fit with reliable Rietveld profile parameters is obtained. The programme has the ability to exercise multi-phase refinement and also to carryout magnetic structure refinement, in the case of neutron diffraction data of magnetic samples.

2.4 The Rietveld refinement method

The principle goal of this method is to refine crystal structures and profiles; the things actually being refined are parameters in modes for the structure and for other specimen and instrument effects on the diffraction pattern.

In the Rietveld method, the least-squares refinements are carried out until the best fit is obtained between the entire observed powder diffraction pattern taken as a whole and the entire calculated pattern based on the simultaneously refined models for the crystal

structure, diffraction optic effects, instrumental factors, and other specimen characteristics (e. g., lattice parameters) as may be desired and can be modelled [33].

For a Rietveld refinement, it is essential that the powder diffraction data be collected properly. The data are recorded in digitized form i.e., as a numerical intensity value, y_2, at each of the several thousand equal increments (steps) i, in the pattern. Depending on the method, the increments can be scattering angle, 2θ or wavelength (x-ray data collected with an energy dispersive detector and an incident beam of 'white' x-radiation). For constant wavelength data, the increments are usually steps in the scattering angle and the intensity y_i at each step i in the pattern is measured directly with a quantum detector on a diffractometer. Factors affecting the data collection that are taken into consideration before the collection are: the geometry of the diffractometer, the quality of the instrument alignment and calibration, the most suitable radiation (e.g. conventional x-ray, synchrotron x-ray or neutron), the wavelength, appropriate sample preparation and thickness, slit sizes and necessary counting time.

The typical step sizes range from 0.01 to 0.05 in 2θ for a fixed wavelength x-ray data and a bit larger for fixed wavelength neutron data. To ensure good counting statistics throughout an x-ray powder diffraction pattern, more time should be spent on data collection at high angles where the intensities are lower. An appropriate data-collection strategy depends on the nature of the

samples (e.g., how well it scatters, how quickly the pattern degrades, peak-broadening effects and the degree of peak overlap). Ideally the step size =FWHM/5, FWHM=full width at half maximum, as there are at least five steps across the top of each peak. The time per step should approximately compensate for the gradual decline in intensity with 2θ.

Rietveld refinement with neutron diffraction data has been notably successful with both fixed-wavelength (K_1 & K_2) data. The Rietveld method is the same no matter what powder diffraction data are used. The differences among data sources affected the data preparation that is required, whether the steps are in angle or energy, and the instrumental parameters that are refined but not in the method itself.

In all cases, the best fit sought is the best least square fit to all of the thousands of y_i's simultaneously [34]. The quantity minimized in the least square refinement is the residual, S_y:

$$S_y = \sum_i w_i (y_i - y_{ci})^2 \quad \text{.....(2.2)}$$

where,

$w_i = 1/y_i$

y_i = Observed (gross) intensity at the i^{th} step.

y_{ci} = Calculated intensity at the i^{th} step.

and the sum is over all data points.

A powder diffraction pattern of a crystalline material may be thought of as a collection of individual reflection profiles, each of which has a peak height, a peak position, a breadth, tails which decay gradually with distance from peak positions, and an integrated area which is proportional to the Bragg intensity, I_k, where k stands for the Miller indices, h, k, l. I_k is proportional to the square of the absolute value of the structure factor $|F|^2$. It is a crucial feature of the Rietveld method that no effort is made in advance to allocate the observed intensity to particular Bragg reflections or to resolve the overlapping reflections. Consequently, a reasonably good starting model is needed. The 'method is a structure refinement method'. Typically, many Bragg reflections contribute to the intensity, y_i, observed at any arbitrarily chosen point, i, in the pattern. The calculated intensities y_{ci}, are determined from the $|F_K|^2$ values, calculated from the structural model by summing the calculated contributions from neighbouring (i.e., within a specified range) Bragg reflections plus the background:

$$y_{ci} = s\sum_k L_k |F_k|^2 \phi(2\theta_i - 2\theta_k) P_k A + y_{bi} \quad \text{.....(2.3)}$$

where, s is scale factor, k refers to the Miller indices, h, k, l for the Bragg reflection, L_k is the Lorentz polarization, and multiplicity factors. ϕ is the reflection profile function, P_k is the preferred orientation

function, A is an absorption factor, F_k is the structure factor for the k^{th} Bragg reflection and y_{bi} is the background intensity at the i^{th} step. The structure factor F_k, is given by

$$F_k = \sum_j N_i f_i \exp\left[2i\left(hx_j + ky_j + lz_j\right)\right]\exp\left[-M_j\right] \quad \text{.....(2.4)}$$

with $M_j = 8^2 u_s^{-2} \sin^2 l^2$, where u_s^{-2} is the root-mean square thermal (and random static) displacement of the j^{th} atom.

The effective absorption factor, A, differs with instrument geometry. It is usually taken to be a constant for the instrument geometry used for the x-ray diffractometer. The least squares minimization procedures lead to a set of *normal equations* involving derivatives of all of the calculated intensities, y_{ci}, with respect to each adjustable parameters and are solvable by inversion of the *normal matrix* with element M_{jk} formally given by

$$M_{jk} = \sum_i 2w\left[\left(y_i - y_{ci}\right)\frac{\partial^2 y_{ci}}{\partial x_j \partial x_k} - \left(\frac{\partial y_{ci}}{\partial x_j}\right)\left(\frac{\partial y_{ci}}{\partial x_k}\right)\right] \quad \text{.....(2.5)}$$

where the parameters x_j, x_k are (same set) adjustable parameters. In the use of this algorithm, it is common practice to approximate these matrix elements by deletion of the first term, that in $(y_i\text{-}y_{ci})$. Thus we are dealing with the creation and inversion of an m X m matrix, where m is the number of parameters being refined. Because the residual function

is non-linear, the solution must be found with an iterative procedure in which the shifts, x_k are

given by

$$x_k = \sum_j M_{jk}^{-1} \frac{\partial s_y}{\partial x_k} \quad \text{.....(2.6)}$$

The calculated shifts are applied to the initial parameters to produce, a supposedly, improved model and the whole procedure is then repeated. Because the relationships between the adjustable parameters and the intensities are non-linear, the starting model must be close to the correct model or the non-linear least squares procedure will not lead to the global minimum.

The model parameters that may be refined to include not only atomic position, thermal, and site-occupancy parameters but also parameters for the background, lattice, instrumental geometrical optical features, specimen aberrations (e.g., specimen displacement and transparency), an amorphous component and specimen reflection-profile-broadening agents such as crystallite size and microstrain. Multiple phases may be refined simultaneously and comparative analysis of the separate overall scale factors for the phases offers what is probably the most reliable current method for doing quantitative

phase analysis. The usual refinable parameters are listed in following table.

Parameters refinable simultaneously during Rietveld refinement

Parameters to be refined for each phase present	**Global parameters**
x_j, y_j, z_j B_j N_j; x_j y_j z_j are position coordinates, B_j is an isotropic thermal parameter and N_j is the site-occupancy multiplier, all for the j^{th} atom in the unit cell	2- Zero shift
Scale factor	Instrumental profile
Specimen-profile breadth parameters	Profile asymmetry
Lattice parameters	Background
Overall temperature factor (thermal parameters)	Wavelength
Individual anisotropic thermal parameters	Specimen displacement
Preferred orientation	Specimen transparency

Crystalline size and microstrain Absorption

Extinction

There are usually two approaches to deal with the background in the powder diffraction pattern. It can be estimated by linear interpolation between selected peak points, and then subtracted, or it can be modelled by an empirical or semi-empirical function containing several refinable parameters. For refining the background, y_{bi} must be obtained from a refinable background function, which may be phenomenological or, better, based on physical reality and include refinable models. One such phenomenological fifth-order polynomial provided with an operator-specific origin is

$$y_{bi} = \sum_{m=0}^{5} B_m \left[\left(2\theta_i / BKPOS \right) - 1 \right]^m \quad \text{.....(2.7)}$$

where BKPOS is the origin that is to be specified in the input control file.

With a complete structure model and good starting values for the background contribution, the unit cell parameters and the profile parameters, the Rietveld refinement of structural parameters can begin. Because the global minimum of the least-square residual function is much shallower with powder data than it is with single-crystal data, and

false minima are more prevalent, the refinement needs constant monitoring. A refinement of a structure of medium complexity can require several hundred cycles. The profile fit is best seen in a plot but can also be followed numerically with a reliability factor or R factor. The difference plots indicate whether a high R-value is due to a profile-parameter problem (i. e., total intensity is approximately correct but there are differences in the peak form) or to a deficiency in the structural model (i.e., integrated intensity does not match). An approximate strategy for refinement can be formulated as the following. Changes in positional parameters cause changes in structure-factor magnitudes and therefore in relative peak intensities, whereas atomic displacement (thermal) parameters have the effect of emphasizing the high-angle region (smaller thermal parameters) or de-emphasizing it (larger thermal parameters).

The scale, the occupancy parameters and the thermal parameters are highly correlated with one another, and are more sensitive to the background correction than are the positional parameters.

The structure should be refined to convergence. That is, the maximum shift estimated standard deviation (e.s.d.) in the final cycle of refinement should be no more than 0.10. All parameters (profile and structural) should be refined simultaneously to obtain correct estimated standard deviation.

R-values

Although a difference profile plot is probably the best way of following and guiding a Rietveld refinement, the fit of the calculated pattern to the observed data can also be given numerically. This is usually done in terms of agreement indices or R-values.

The weighted-profile R-value, R_{wp}, is defined as:

$$R_{wp} = \left[\sum_i^N w_i \{y_i(obs) - y_i(calc)\}^2 / \sum_i^N w_i \{y_i(obs)\}^2 \right]^{1/2} \quad \text{.....(2.8)}$$

where $y_i(obs)$ is the observed intensity at step i, $y_i(calc)$ the calculated intensity, and w_i the weight. From a purely mathematical point of view, R_{wp} is the most meaningful of these R 's because the numerator is the residual being minimized. For the same reason, it is also the one that best reflects the progress of the refinement. Ideally, the final R_{wp} should approach the statistically expected R-value, R_{exp},

$$R_{\exp} = \left[(N - P) / \sum_i^N w_i y_i(obs)^2 \right]^{1/2} \quad \text{.....(2.9)}$$

where N is the number of observations and P the number of parameters. R_{exp} reflects the quality of the data (i.e., the counting statistics). Thus the ratio between the two is another useful numerical criterion, called the goodness of fit. It is generally given as, χ^2 and expressed as:

$$\chi^2 = R_{wp} / R_{\exp} \quad \text{.....(2.10)}$$

If the data have been 'Over-collected', R_{exp} will be very small and χ^2 for a fully refined structure much larger than 1. Conversely, if the data have been 'under-collected', R_{exp} will be larger and χ^2 could be less than 1.

A R-value similar to that reported for single-crystal refinements, based on the agreement between the observed and calculated structure factors, F_{hkl}, can also be calculated by distributing the intensities of the overlapping reflections according to the structure model,

$$R_F = \sum_{hkl} |F_{hkl}(obs) - F_{hkl}(calc)| / \sum_{hkl} |F_{hkl}(obs)| \quad \text{.....(2.11)}$$

Similarly, the Bragg-intensity R-value,

$$R_B = \sum_{hkl} |I_{hkl}(obs) - I_{hkl}(calc)| / \sum_{hkl} |I_{hkl}(obs)| \quad \text{.....(2.12)}$$

where $I_{hkl} = mF^2_{hkl}$ (m = multiplicity), or its weighted equivalent can be used to monitor the improvement in the structure model. Because 'R-Bragg *(R_B)*' and 'R-structure factor *(R_F)*' are based not on actually observed Bragg intensities but on those deduced with the help of the model, they are biased in favour of the model being used. Nonetheless,

they are the R's that are most nearly comparable to the conventional R-values quoted in the literature on single crystal structure refinements. They also serve a useful function because they are insensitive to misfits in the pattern that do not involve the Bragg intensities of the phase(s) being modelled.

R-values are useful indicators for the evaluation of a refinement, especially, in the case of small improvements to the model, but they should not be over interpreted. The most important criteria for judging the quality of a Rietveld refinement are: The fit of the calculated pattern to the observed data and the chemical sense of the structure model.

The former can be evaluated on the basis of the final profile plot (using the complete range of data collected) and the latter on a careful examination of the final atomic positions.

.

In the present work, the fitting was carried out on the samples $Pr_{1.85}Ce_{0.15}Cu_{1-x}Ni_xO_4$ (x = 0.01, x=0.0075, x=0.005, x=0.0025) with space group I4/mmm. The patterns matched very well, giving reliable χ^2 and R-values.

2. 4. 1 Transport properties

Resistivity measurements

Resistivity studies on the high temperature superconducting samples $Pr_{1.85}Ce_{0.15}Cu_{1-x}Ni_xO_4$ (x = 0.01, x=0.0075, x=0.005, x=0.0025) were carried out using the standard. four-probe technique, in

the temperature range 4.2-300K in a cryostat (CTI-8200). These studies show that of Ni doping concentrations x=0.0075 and x=0.01 behave as superconductors with the substantial fall in the transition temperature. However, for x=0.0025 and x=0.005 the superconducting state was not observed. When the sample resistance is measured by two probes using a multimeter, the contact and lead wire resistances cannot be avoided. The four-probe method is a simple technique to overcome this limitation. In this configuration, the lead resistance of the potential leads does not come into the picture because no current flows through these leads under null condition, thus ensuring that the measured potential is the potential of the sample only.

Four contacts were made on a well-sintered pellet using conductive solder of low melting point. Fine enamelled copper wires were used to pass the constant current of the order of few microamperes through the outer two leads using a constant current source. The voltage developed across the two inner leads was measured using the nanovoltmeter as a function of temperature. The resistivity as a function of temperature was measured during the warming up cycle. The characteristic parameters associated with the superconducting transition temperature generally used are: superconducting onset temperature, the temperature at which resistance goes to zero within the measuring capability of measuring instrument, the temperaure corresponding to the mid-point of the superconducting transition and the width of the superconducting transition.

The block diagram of the four-probe setup used for measuring the resistivity is shown in Fig.2.5

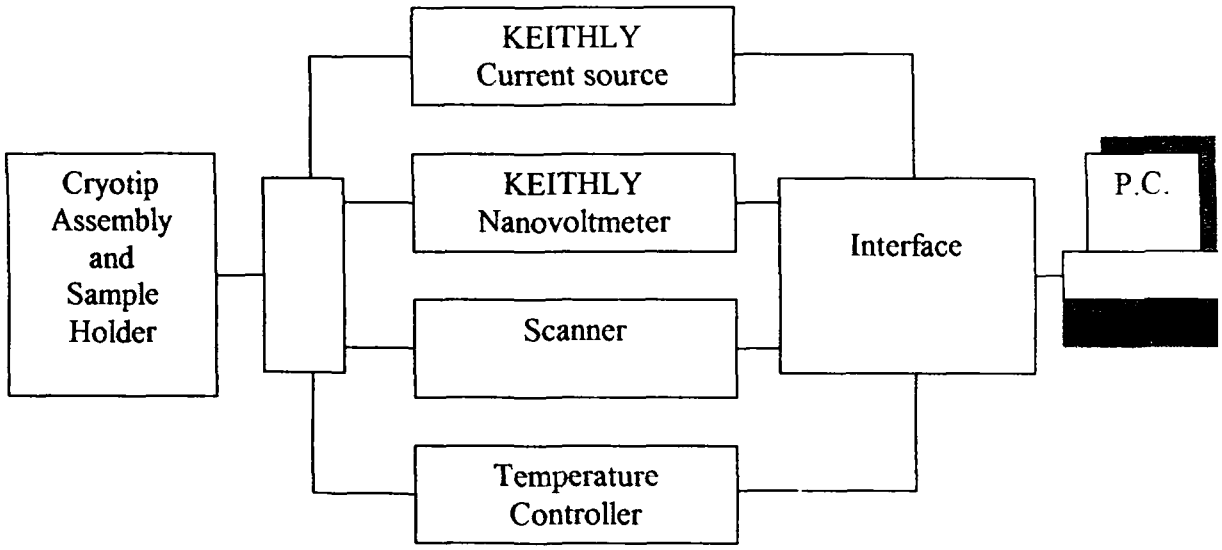

Figure 2.5 Block-diagram of four-probe resistivity setup.

Chapter III

Results and Discussion

Introduction

In this chapter, we discuss the interpretation of our studies on the structural and transport aspects of $Pr_{1.85}Ce_{0.15}Cu_{1-x}Ni_xO_4$ (x = 0.01, 0.0075, 0.005, 0.0025) superconducting samples. The powder x-ray diffraction (XRD) patterns of whole series of $Pr_{1.85}Ce_{0.15}Cu_{1-x}Ni_xO_4$ have been recorded at room temperature. The lattice parameters and the unit cell volume of all the samples have been calculated. The temperature dependence of electrical resistivity of the samples with different Ni concentrations has also been measured in the temperature range 4.2-300K.

3.1 The Structural Analysis (Bulk Samples)

To study the structure of the of $Pr_{1.85}Ce_{0.15}Cu_{1-x}Ni_xO_4$ samples, we have performed the powder XRD measurement at room temperature and fitted the XRD patterns using FULLPROF code for Rietveld analysis of these samples. Figs. 3.2, 3.3, 3.4 and 3.5 show experimental and calculated XRD patterns using Rietveld technique respectively for x = 0.01, 0.0075, 0.005, and 0.0025 samples. The analysis of the XRD patterns show that all the samples are formed in single-phase with the T´-crystal symmetry and space group *I4/mmm*. It is to be mentioned here that the lattice parameters of $Pr_{2-x}Ce_xCuO_4$ change considerably with Ni doping. The variation of the lattice parameters and the

unit cell volume with Ni concentration are shown in Fig.3.1. The values of parameters *a* and *b* decrease from 3.96268 to 3.93775 Å with the increase of Ni concentration. However, the parameter *c* shows very small irregular variation. The unit cell volume decreases with increase in the Ni concentration (Fig.3.1), obviously due to the size mismatch of Cu and Ni ions. We summarize all these observations in Table 3.1.

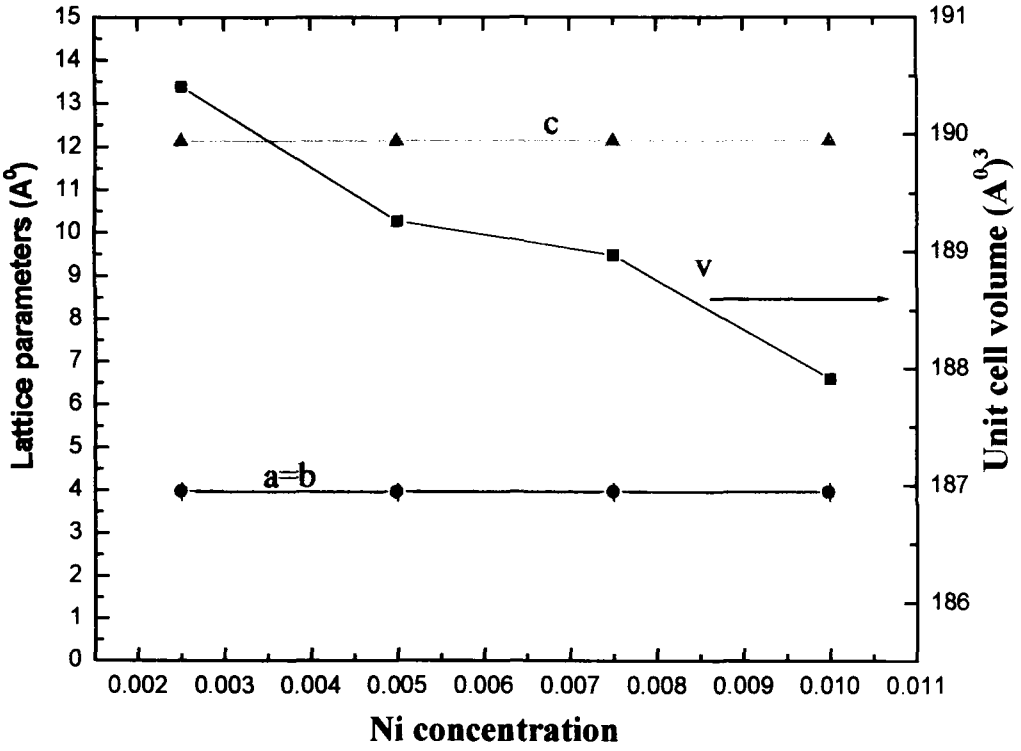

Fig.3.1 The variation of the lattice parameters and unit cell volume with Ni concentration

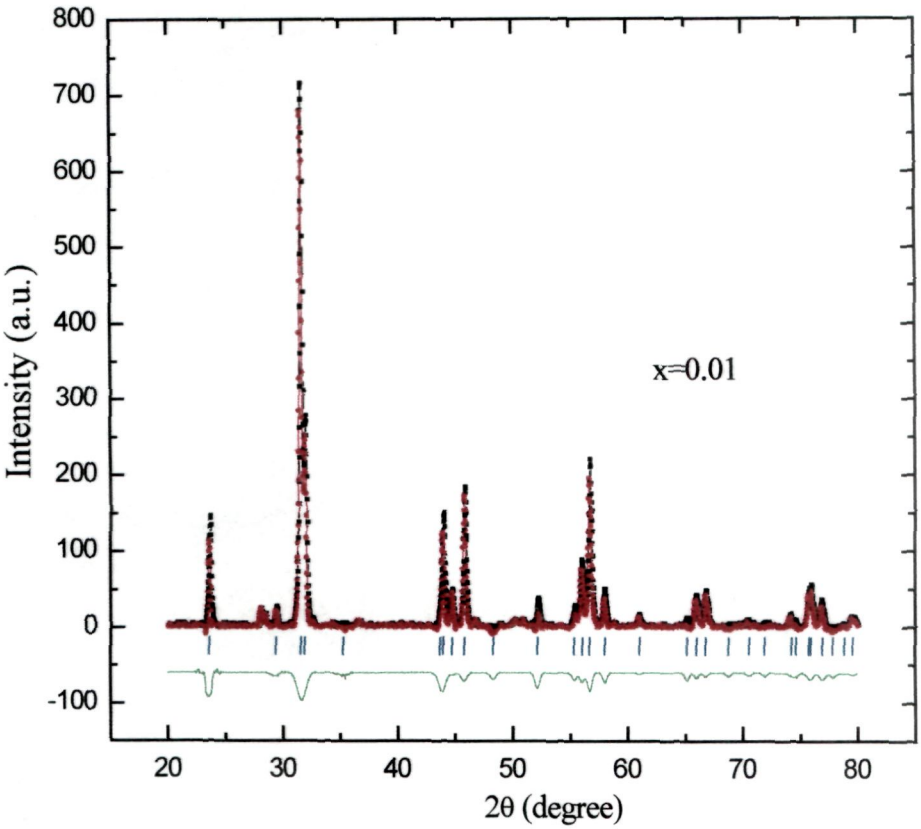

Fig. 3.2 XRD pattern of the compound $Pr_{1.85}Ce_{0.15}Cu_{0.99}Ni_{0.01}O_4$. *Black dots plus line indicate the experimental data and calculated profile is the red dots plus line overlying them. The lowest curve shows the difference between experimental and calculated patterns. The vertical bars indicate the expected reflection positions.*

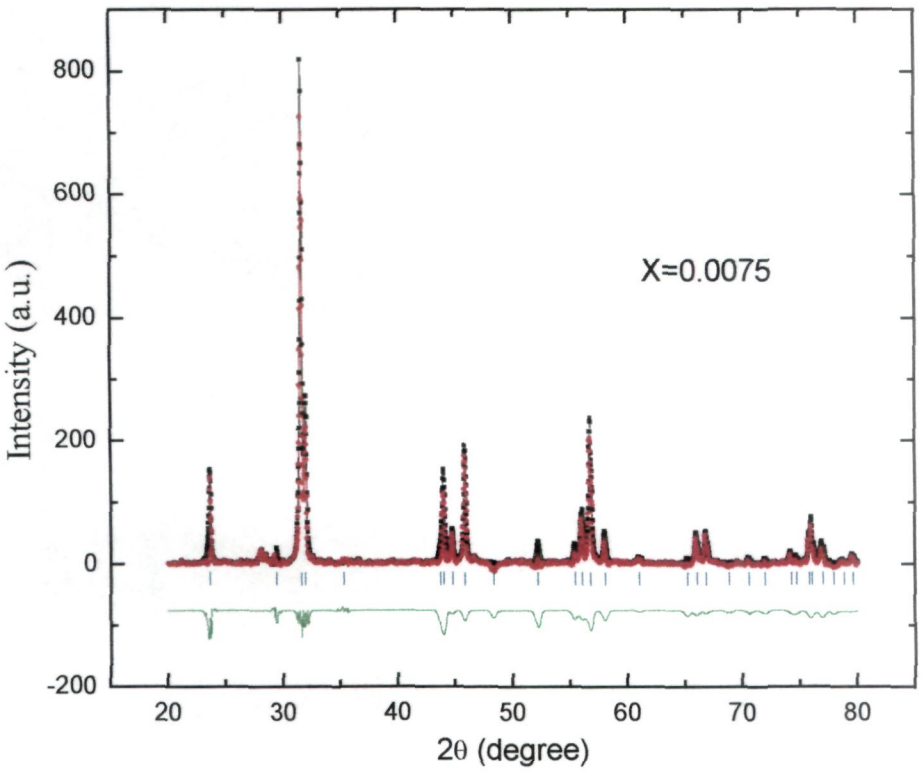

Fig. 3.3 XRD pattern of the compound $Pr_{1.85}Ce_{0.15}Cu_{0.9925}Ni_{0.0075}O_4$. *Black dots plus line indicate the experimental data and calculated profile is the red dots plus line overlying them. The lowest curve shows the difference between experimental and calculated patterns. The vertical bars indicate the expected reflection positions.*

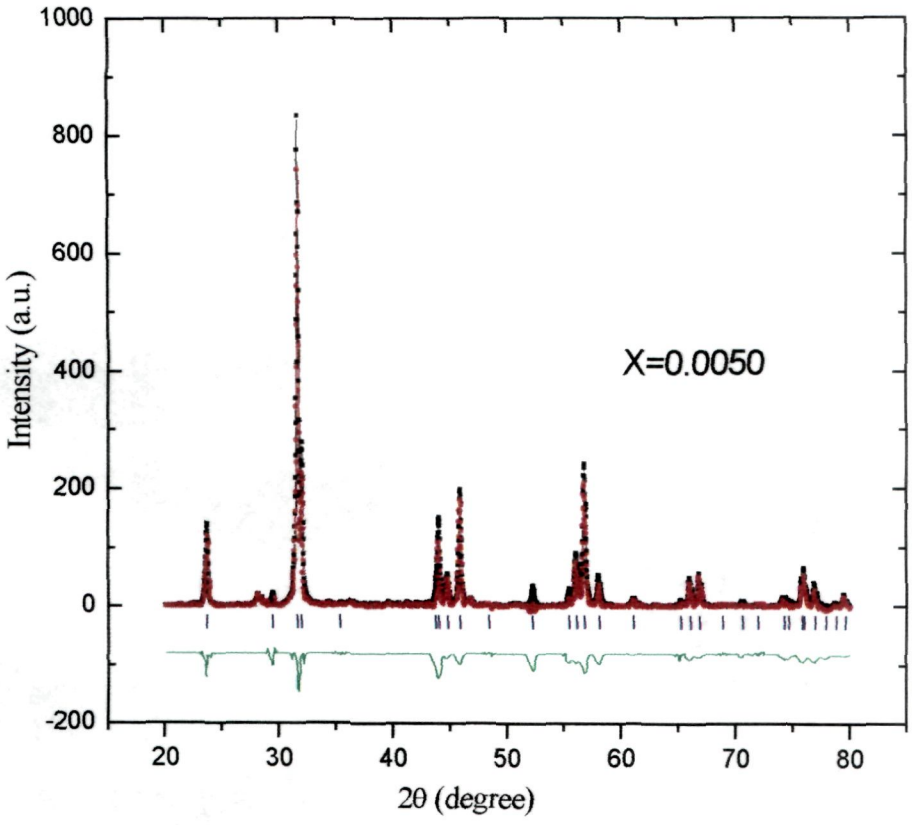

Fig. 3.4 XRD pattern of the compound $Pr_{1.85}Ce_{0.15}Cu_{0.995}Ni_{0.005}O_4$. *Black dots plus line indicate the experimental data and calculated profile is the red dots plus line overlying them. The lowest curve shows the difference between experimental and calculated patterns. The vertical bars indicate the expected reflection positions.*

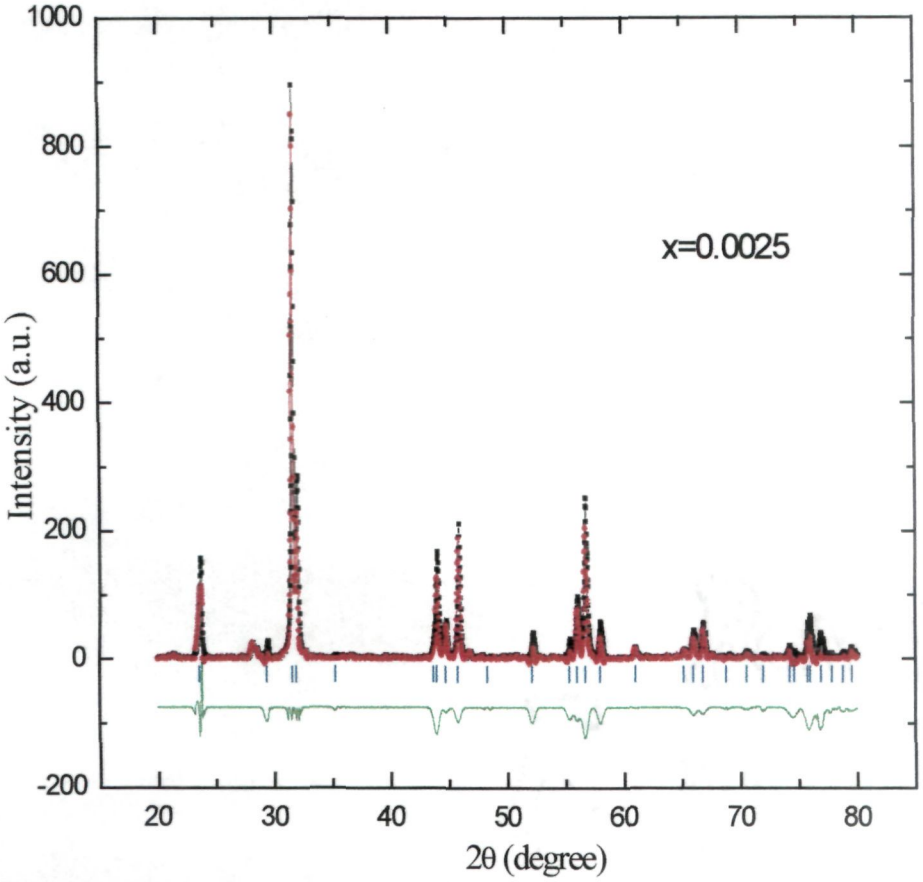

Fig. 3.5 XRD pattern of the compound $Pr_{1.85}Ce_{0.15}Cu_{0.9975}Ni_{0.0025}O_4$. *Black dots plus line indicate the experimental data and calculated profile is the red dots plus line overlying them. The lowest curve shows the difference between experimental and calculated patterns. The vertical bars indicate the expected reflection positions.*

Table 3.1 The lattice parameters and the unit cell volume for different compositions of $Pr_{1.85}Ce_{0.15}Cu_{1-x}Ni_xO_4$.

Composition	*Crystal Symmetry*	*a (Å)*	*b (Å)*	*c (Å)*	*Unit cell volume ($Å^3$)*
$Pr_{1.85}Ce_{0.15}Cu_{0.9975}Ni_{0.0025}O_4$	Tatragonal	3.96268	3.96268	12.12596	190.41
$Pr_{1.85}Ce_{0.15}Cu_{0.995}Ni_{0.005}O_4$	Tatragonal	3.9512	3.9512	12.12315	189.26
$Pr_{1.85}Ce_{0.15}Cu_{0.9925}Ni_{0.0075}O_4$	Tatragonal	3.9482	3.9482	12.12315	188.97
$Pr_{1.85}Ce_{0.15}Cu_{0.99}Ni_{0.01}O_4$	Tatragonal	3.93775	3.93775	12.12172	187.95

We have fitted all lattice parameters shown in Table-3.1 with the help of powder X-ray software available for the fitting of the lattice parameters. The maximum deviation that occurred between the observed and calculated values of the interplanar spacing (*d* value) remains below 0.09176 Å, while in most of the cases there is hardly any difference between the two values. The observed and calculated *d* values at different 2θ values for $Pr_{1.85}Ce_{0.15}Cu_{1-x}Ni_xO_4$ (x = 0.01, 0.0075, 0.005, 0.0025) are tabulated in Tables 3.2 to 3.5

Table 3.2 The observed and calculated interplanar distances at different 2θ values for $Pr_{1.85}Ce_{0.15}Cu_{0.9975}Ni_{0.0025}O_4$.

S.N.	*hkl*	2θ (degrees)	θ (degrees)	$d_{obs.}$(Å)	$d_{cal.}$(Å)	diff. (Å)
1	003	23.638	11.819	3.76077	3.81167	-0.0509
2	110	28.106	14.053	3.17227	3.14896	0.02331
3	111	29.401	14.7005	3.03547	3.03595	-0.00048
4	004	31.603	15.8015	2.8288	2.85875	-0.02995
5	202	43.971	21.9855	2.05756	2.07486	-0.0173
6	105	44.739	22.3695	2.024	2.03441	-0.01041
7	210	45.826	22.913	1.97852	1.99158	-0.01306
8	106	52.18	26.09	1.75154	1.75212	-0.00058
9	214	56.019	28.0095	1.64026	1.63412	0.00614
10	116	56.703	28.3515	1.6221	1.63047	-0.00837
11	205	57.973	28.9865	1.58955	1.59539	-0.00584
12	222	60.967	30.4835	1.51846	1.51797	0.00049
13	310	65.939	32.9695	1.41549	1.40826	0.00723
14	311	66.776	33.388	1.39976	1.3977	0.00206
15	009	74.148	37.074	1.27777	1.27056	0.00721
16	305	75.94	37.97	1.25201	1.24514	0.00687
17	320	76.827	38.4135	1.23975	1.23512	0.00463
18	322	79.435	39.7175	1.20547	1.20727	-0.0018
19	218	83.409	41.7045	1.15784	1.16125	-0.00341
20	317	92.628	46.314	1.06522	1.06663	-0.00141
21	412	93.197	46.5985	1.06021	1.06131	-0.0011
22	229	102.142	51.071	0.99019	0.98877	0.00142

Table 3.3 The observed and calculated interplanar distances at different 2θ values for $Pr_{1.85}Ce_{0.15}Cu_{0.995}Ni_{0.005}O_4$.

S.N.	*hkl*	2θ (degrees)	θ (degrees)	$d_{obs.}$(Å)	$d_{cal.}$(Å)	diff. (Å)
1	003	23.64676	11.82338	3.76137	3.85313	-0.09176
2	110	29.41252	14.70626	3.03552	3.05675	-0.02123
3	103	31.60542	15.80271	2.82965	2.87637	-0.04672
4	105	43.97276	21.98638	2.05804	2.03865	0.01939
5	202	44.75354	22.37677	2.02392	2.02451	-0.00059
6	106	52.20068	26.10034	1.75128	1.75972	-0.00844
7	116	56.01316	28.00658	1.64075	1.62985	0.0109
8	116	56.71454	28.35727	1.62211	1.62985	-0.00774
9	205	57.98836	28.99418	1.58946	1.57888	0.01058
10	223	65.94218	32.97109	1.41566	1.42069	-0.00503
11	302	66.78322	33.39161	1.39986	1.39817	0.00169
12	217	75.9506	37.9753	1.25203	1.25563	-0.0036
13	314	76.84094	38.42047	1.23973	1.23573	0.004
14	208	79.44236	39.72118	1.20553	1.20123	0.0043
15	218	83.42792	41.71396	1.15776	1.15738	0.00038
16	325	92.63492	46.31746	1.06527	1.06434	0.00093
17	402	93.2026	46.6013	1.06026	1.06231	-0.00205

Table 3.4 The observed and calculated interplanar distances at different 2θ values for $Pr_{1.85}Ce_{0.15}Cu_{0.9925}Ni_{0.0075}O_4$.

S.N.	*hkl*	2θ (degrees)	θ (degrees)	$d_{obs.}$(Å)	$d_{cal.}$(Å)	diff (Å)
1	105	23.63816	11.81908	2.01012	1.9953	0.01482
2	210	28.09604	14.04802	1.96532	1.97021	-0.00489
3	213	29.4001	14.70005	1.7413	1.74211	-0.00089
4	214	31.60326	15.80163	1.61333	1.61082	0.00251
5	205	43.9637	21.98185	1.58131	1.5699	0.01141
6	302	44.74282	22.37141	1.40934	1.4204	-0.01106
7	310	45.8287	22.91435	1.39369	1.39315	0.00054
8	118	52.1878	26.0939	1.27364	1.27602	-0.00238
9	314	56.71658	28.35829	1.2474	1.24707	0.00033
10	217	57.98146	28.99073	1.23535	1.24136	-0.00601
11	109	65.94092	32.97046	1.20082	1.19659	0.00423
12	306	66.78308	33.39154	1.15401	1.15377	0.00024
13	227	74.10626	37.05313	1.11148	1.11559	-0.00411
14	410	75.94826	37.97413	1.07088	1.0685	0.00238
15	403	76.82866	38.41433	1.05737	1.05629	0.00108
16	105	79.48174	39.74087	2.01012	1.9953	0.01482
17	210	83.42572	41.71286	1.96532	1.97021	-0.00489
18	213	87.41984	43.70992	1.7413	1.74211	-0.00081
19	214	91.67298	45.83649	1.61333	1.61082	0.00251
20	205	93.19946	46.59973	1.58131	1.5699	0.01141

Table 3.5 The observed and calculated interplanar distances at different 2θ values for $Pr_{1.85}Ce_{0.15}Cu_{0.99}Ni_{0.01}O_4$.

S.N.	*hkl*	2θ (degrees)	θ (degrees)	$d_{obs.}$(Å)	$d_{cal.}$(Å)	diff (Å)
1	003	23.6464	11.8232	3.7555	3.76023	-0.00473
2	110	28.11202	14.05601	3.16881	3.14884	0.01997
3	111	29.42242	14.71121	3.03071	3.0329	-0.00219
4	004	31.61324	15.80662	2.82567	2.82017	0.0055
5	202	43.9792	21.9896	2.05607	2.07104	-0.01497
6	105	44.74998	22.37499	2.02245	2.01258	0.00987
7	210	45.84016	22.92008	1.97688	1.9915	-0.01462
8	204	52.19468	26.09734	1.75029	1.74756	0.00273
9	214	56.01876	28.00938	1.63958	1.62678	0.0128
10	214	56.72572	28.36286	1.62082	1.62678	-0.00596
11	205	57.9822	28.9911	1.58867	1.58477	0.0039
12	222	60.97444	30.48722	1.51771	1.51645	0.00126
13	117	65.18378	32.59189	1.42955	1.43457	-0.00502
14	008	65.93408	32.96704	1.41509	1.41009	0.005
15	311	66.79306	33.39653	1.39897	1.39736	0.00161
16	118	74.14624	37.07312	1.27742	1.28694	-0.00952
17	217	75.95704	37.97852	1.25141	1.25275	-0.00134
18	305	76.84058	38.42029	1.23922	1.24005	-0.00083
19	109	79.43644	39.71822	1.20513	1.20653	-0.0014
20	218	83.42608	41.71304	1.15736	1.15082	0.00654
21	400	87.38568	43.69284	1.11483	1.11328	0.00155
22	411	91.65844	45.82922	1.0737	1.07513	-0.00143
23	317	93.2063	46.60315	1.0599	1.06039	-0.00049

3.2 Transport Analysis (Bulk Samples)

The electrical transport behaviour of $Pr_{1.85}Ce_{0.15}Cu_{1-x}Ni_xO_4$ superconducting samples has been investigated. The pure Pr_2CuO_4 sample is semiconducting in nature showing the resistivity around MΩ-cm at room temperature (300 K) [3]. The highest superconducting transition temperature (T_c ~ 25 K) of this series is for Ce ~ 0.15. Fig.3.6 shows the resistivity as a function of temperature for the samples with x = 0.0025, 0.005, 0.0075 and 0.01. It is clearly evident from the Figure that there is a substantial fall in transition temperature at the doping concentrations of 0.0025 and 0.0050 with transition temperatures 16.863K and 13.244K respectively. However, the superconductivity is destroyed at the doping concentration of 0.0075 and 0.0100. Actually, the magnetic Ni introduces the magnetic impurity in the base superconducting material ($Pr_{1.85}Ce_{0.15}CuO_4$). The increase of Ni impurity leads to the fall of T_c. So after a critical concentration (0.005), it looses its superconducting behaviour and shows semiconducting nature as the pure sample.

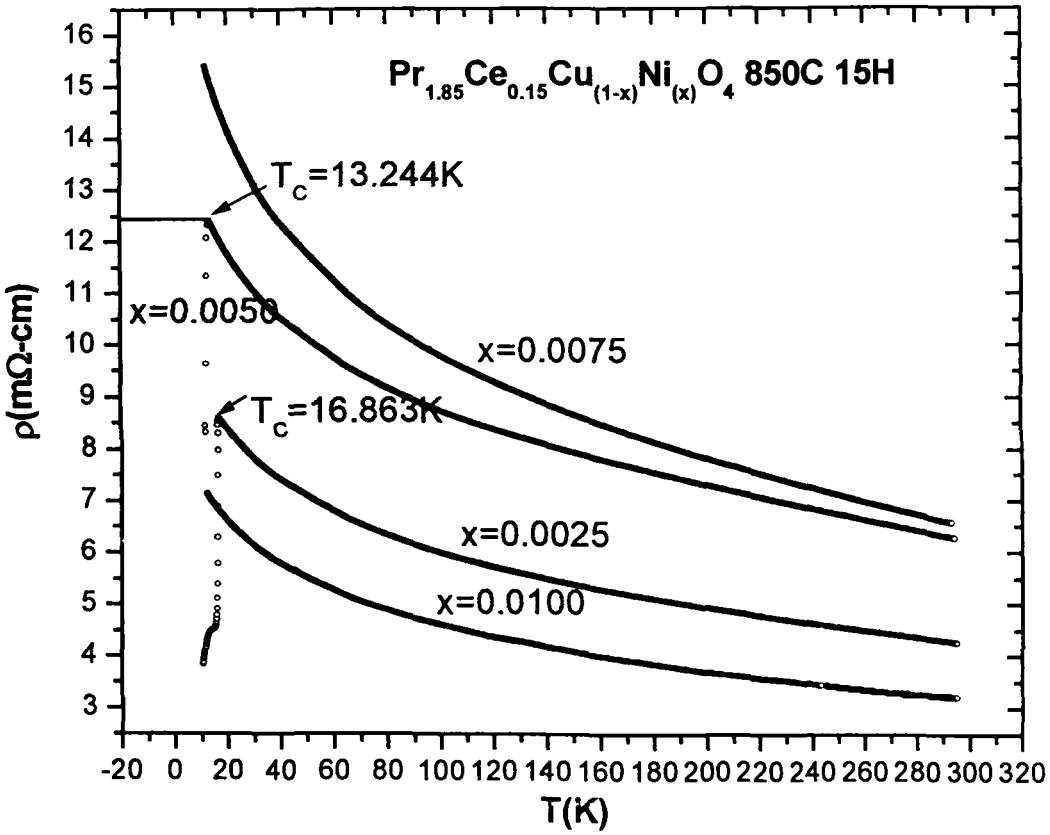

Fig.3.6Temperature dependent resistivity measurements of $Pr_{1.85}Ce_{0.15}Cu_{1-x}Ni_xO_4$

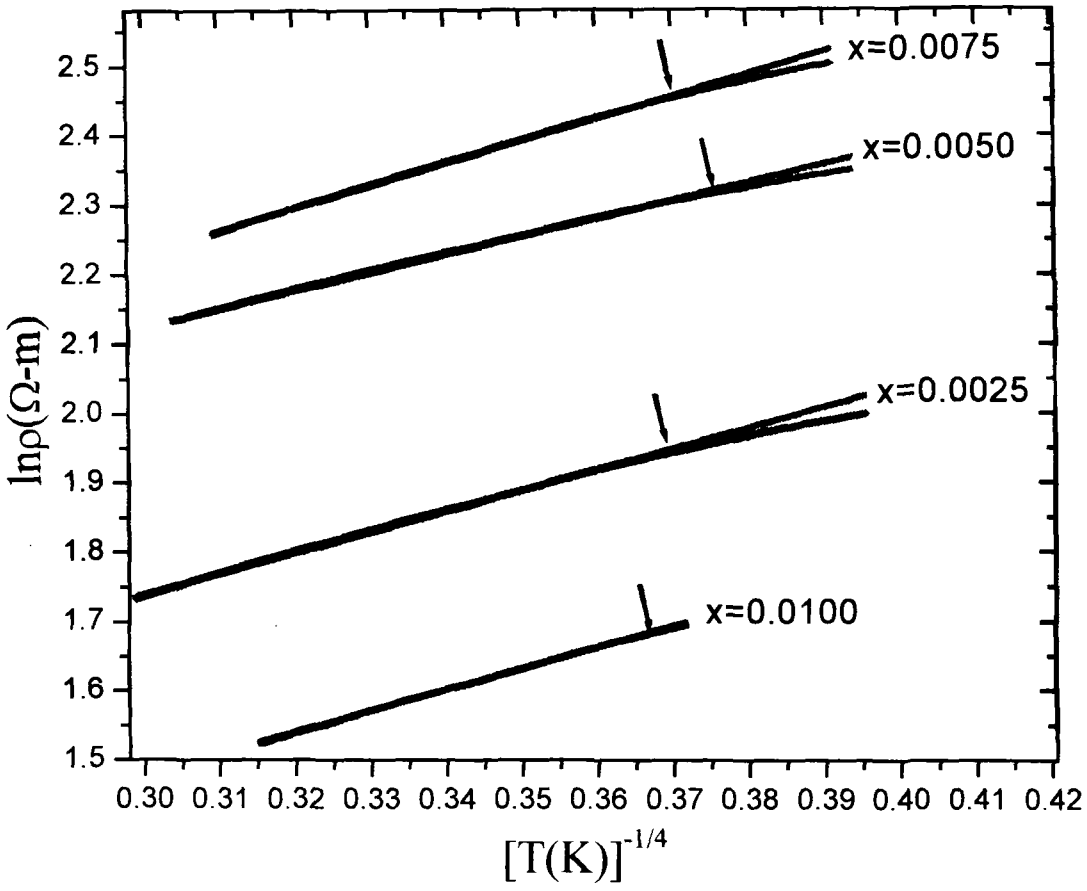

Fig.3.7 Plot of lnρ against $1/T^{1/4}$ *of the resistivity data for samples* $Pr_{1.85}Ce_{0.15}Cu_{1-x}Ni_xO_4$ (x = 0.01, 0.0075, 0.005, 0.0025). *Black line indicates the experimental data, while Red line shows the calculated linear fit in the variable range hopping model.*

To understand the nature of the electrical transport properties in these materials we have attempted to fit the resistivity data as a function of temperature in the Mott's variable range hopping (VRH) model i.e.,

$$\rho(T)=\rho_0 \exp\left[\left(\frac{T_0}{T}\right)^{1/4}\right]$$

where T_0 is a characteristic temperature which is related to the density of states in the vicinity of the Fermi energy $N(E_F)$ and the localization length ξ, i.e.,

$$k_B T_0 \approx 21/\left[\xi^3 N(E_F)\right]$$

Accordingly, we have plotted $ln\ \rho$ vs $T^{-1/4}$ shown in Fig.3.7. It is observed that the resistivity data shows the best fit with the VRH model within the temperature range of 54-300 K for all the compositions with x = 0.0025, 0.005, 0.0075 and 0.01. The slopes of the curves are decreasing with the increase of Ni concentration first for x = 0.0025, 0.005 and then increasing for x = 0.0075 and 0.01. Correspondingly, the activation energy (E_c) also first decreases and then increases as shown in Table 3.6. The increase and decrease of activation energy can explain the resistivity of the samples.

Table 3.6 Resistivity and activation energy for different compositions of $Pr_{1.85}Ce_{0.15}Cu_{1-x}Ni_xO_4$ (x = 0.01, x=0.0075, x=0.005, x=0.0025).

Composition	*T_d	ρ (Ω-m) at T_d	E_c (eV x10^{-5})
$Pr_{1.85}Ce_{0.15}Cu_{0.9975}Ni_{0.0025}O_4$	54.953	6.939	696.45
$Pr_{1.85}Ce_{0.15}Cu_{0.9950}Ni_{0.0050}O_4$	55.126	9.948	393.37
$Pr_{1.85}Ce_{0.15}Cu_{0.9925}Ni_{0.0075}O_4$	54.236	11.568	925.19
$Pr_{1.85}Ce_{0.15}Cu_{0.9900}Ni_{0.0100}O_4$	55.544	5.372	762.90

* The temperature below which VRH model is not applicable.

Chapter IV

Conclusions

Results of our study of the structural and transport properties of Ni doped $Pr_{2-x}Ce_xCuO_4$ samples may be summarized as follows.

4.1 Structural Properties

The XRD measurement at room temperature fitted with Rietveld technique clearly shows that prepared samples are in single phase. The pure $Pr_{2-x}Ce_xCuO_4$ is found to have T´- symmetry with space group I4/mmm. On doping with Ni at the Cu site the lattice parameters change considerably, but doped compounds remain in the T´-symmetry. The unit cell volume decreases with the Ni concentration and reaches a value of 187.95 $Å^3$ for the end member ($Pr_{1.85}Ce_{0.15}Cu_{0.99}Ni_{0.01}O_4$) of the series.

.

4.2 Transport Properties

We measured the temperature dependence of resistivity of, $Pr_{1.85}Ce_{0.15}Cu_{1-x}Ni_xO_4$ (x = 0.01, 0.0075, 0.005, 0.0025) in the temperature range 4.2-300K. It is clearly evident that there is substantial fall in transition temperature at the doping concentration of 0.0025 and 0.0050 with transition temperatures 16.863K and 13.244K respectively. However, superconducting phase vanishes at 0.0100 and 0.0075.Our higher temperature resistivity data fit well in the Mott's variable range hopping (VRH) model in these materials. The fit shows that the slopes of the curves first decrease with the increase of Ni concentration for x = 0.0025, 0.005 and then increase for x = 0.0075

and 0.01. Accordingly, the activation energy (E_c) also first decreases and then increases. The increase and decrease of activation energy can explain the resistivity of the samples.

References

[1] Y.Tokura, H. Takagi, S. Uchida, Nature (London) **337,** (1989) 345.

[2] H. Takagi, S. Uchida, Y.Tokura, Phys. Rev. Lett. **62,**(1989) 1197.

[3] A.Conceicao, C.H.Cohenca, R.F.Jardim, Physica **C 333,**(2000) 170-180.

[4] J.B.Torrance, Y.Tokura, A.I.Nazzal, A.Bezinge, T.C.Huang, S.S.P.Parkin, Phys. Rev. Lett. **61**, (1988)1127.

[5] M.Brinkman, T.Rex, H.Bach, K.Westerholt, Phys.Rev.Lett. **74**, (1995) 4927.

[6] J.L.Peng, E.Maiser, T.Venkatesan, R.L.Greene, C.Czjzek, Phys. Rev. **B 55,** (1997) R(6145).

[7] M.Brinkman, T.Rex, M.Stief, H.Bach, K.Westerholt, Physica **C 269,** (1996) 76.

[8] E.Maiser, P.Fournier, J.L.Peng, F.M.Araujo-Moreira, T.Venkatesan, R.L.Greene, C.Czjzek, Physica **C 297**, (1998) 15.

[9] R. Saez Puche, M. Norton, T. R. White, and W.S. Glaunsinger, Mater. Res. Bull. **17**, 1523 (1982).

[10] Amlan Biswas, P. Fournier, V.N. Smolyaninova, R. C. Budhani, J.S.Higgins, and R.L.Greene, Physical Review **B 64**, (2001)104519.

[11] G.F.Zharkov, Phys. Rev. **B 63**, (2001) 214502.

[12] M.Sigrist, T.M.Rice, Rev.Mod. Phys. **67**, (1995) 503.

[13] J. G. Bednorz and K.A.Müller, Z.Phys. **B 64**, 189(1986).

[14] C.W.Chu, P.H.Hor, R.L.Meng, L.Gao, and Z.J.Haung, Science **235**, 567 (1987).

[15] Maeda, H.Tanoka, Y.Fukutami, M.Asano, T.(1988) Jpn. J.Appl. Phys. **27**: L209.

[16] P.W.Anderson, Science **235**, 1196 (1987).

[17] J.A.Wilson, J. Phys. **C** : Sol. St. Phys. 20 L911(1987).

[18] P.W.Anderson, Matter. Res. Bull. **8**, 153 (1973).

[19] S.A.Kivelson, D.S.Rokhsar, and J.P.Sethna, Phys. Rev. **B 35**, 8865 (1987).

[20] D.G.Thouless, Phys. Rev. **B 36**, 7187 (1987).

[21] C.Verma, S.Schmith-Rink, and E. Abrahams, Sol. St. Comm. **62,** 681 (1987).

[22] V.J. Emery, Phys. Rev.Lett. **58**, 2794 (1987).

[23] R.H.Parmenter, Phys. Rev. Lett. **59**, 923 (1987).

[24] R.A.Barrio, C.Wang, J.Tagüeana-Martinez, D.Rios-Jara, T.Akachi, and R. Escudero, MRS Boston Symp., 801 (1987).

[25] N. F. Mott, J. Non-Cryst. Sol. **1**, 1 (1968).

[26] Vinay Ambegaokar, B. I. Halperin and J. S. Langer, Phys. Rev. **B 4**, 2612 (1971).

[27] B. I. Shklovskii and A. I. Efros, *Electronic Properties of Doped Semiconductors* (Springer-Verlag, Berlin, 1984).

[28] Allen Miller and Elihu Abrahams, Phys. Rev. **120**, 745 (1960).

[29] H.M. Rietveld, Acta. Cryst. **22**, 151 (1967).

[30] H.M. Rietveld, J. Appl. Cryst. **2**, 65 (1969).

Laboratoire Leon Brillouin (CEA-CNRS).

[31] C. Dong, J. Appl. Cryst. **32**, 838 (1999).

[32] Juan Rodriguez-Carvajal (version3.5d oct98-LLB-JRC)

Laboratoire Leon Brillouin (CEA-CNRS).

[33] L.B. McCusker, R. B. Von Dreele, D. E. Cox, D. Louer and P. Scardi, J. Appl. Cryst. **32**, 36 (1999).

[34] A. Yong "The Rietveld Method", IUCr & Oxford Science Publications (1996).